

Dual Tumor-Targeting Nanocarrier System for siRNA Delivery Based on pRNA and Modified Chitosan

Lin Li,¹ Xiaoqin Hu,^{2,4} Min Zhang,^{1,4} Siyu Ma,^{2,4} Fanglin Yu,² Shiqing Zhao,² Nan Liu,¹ Zhiyuan Wang,¹ Yu Wang,³ Hua Guan,³ Xiujie Pan,³ Yue Gao,² Yue Zhang,² Yan Liu,² Yang Yang,² Xuemei Tang,² Mingyuan Li,² Cheng Liu,² Zhiping Li,² and Xingguo Mei²

¹State Key Laboratory of Pathogen and Biosecurity, Beijing Institute of Microbiology and Epidemiology, Beijing 100071, China; ²Beijing Institute of Pharmacology and Toxicology, Beijing 100850, China; ³Beijing Institute of Radiation Medicine, Beijing 100850, China

Highly specific and efficient delivery of siRNA is still unsatisfactory. Herein, a dual tumor-targeting siRNA delivery system combining pRNA dimers with chitosan nanoparticles (CNPPs) was designed to improve the specificity and efficiency of siRNA delivery. In this dual delivery system, folate-conjugated and PEGylated chitosan nanoparticles encapsulating pRNA dimers were used as the first class of delivery system and would selectively deliver intact pRNA dimers near or into target cells. pRNA dimers simultaneously carrying siRNA and targeting aptamer, the second class of delivery system, would specifically deliver siRNA into the target cells via aptamer-mediated endocytosis or proper particle size. To certify the delivering efficiency of this dual system, CNPPs, pRNA dimers alone, chitosan nanoparticles containing siRNA with folate conjugation and PEGylation (CNPS), and chitosan nanoparticles containing pRNA dimers alone (CN) were first prepared. Then, we observed that treatment with CNPPs resulted in increased cellular uptake, higher cell apoptosis, stronger cell cytotoxicity, and more efficacious gene silencing compared to the other three formulations. Higher accumulation of siRNA in the tumor site, stronger tumor inhibition, and longer circulating time were also observed with CNPPs compared to other formulations. In conclusion, this dual nanocarrier system showed high targeting and favorable therapeutic efficacy both in vitro and in vivo. Thereby, a new approach is provided in this study for specific and efficient delivery of siRNA, which lays a foundation for the development of pRNA hexamers, which can simultaneously carry six different substances.

INTRODUCTION

RNAi, a potent and highly specific gene-silencing phenomenon triggered by double-stranded RNA helix,¹ has emerged as a promising strategy for treatment of a wide range of diseases.² Small interfering RNA (siRNA) with 21–23 base pairs has been proven to be more efficient in gene silencing than other RNAi molecules and opens wide perspectives in therapeutics for the treatment of many diseases linked to elevated expression of identified genes, including cancer and infectious, inflammatory, and neurodegenerative diseases.^{3,4} As a result,

several clinical trials using siRNA approaches have been conducted in patients with liver cancers and metastatic melanoma.^{2,5,6} Although a promising application shown in the treatment of diseases, the poor physicochemical properties of siRNA, such as hydrophilicity, high molecular weight, negative charge, the resultant poor cell penetration, and instability in physiological fluids hinder its ultimate functionality in the clinic when administered as a naked molecule.³ Therefore, an effective delivery system is required for siRNA to overcome these challenges and reach the target cells.^{4–6}

An ideal vector for siRNA delivery should exhibit the following characteristics: (1) should be biocompatible, non-immunogenic, and have low toxicity; (2) the size should be below 200 nm with an optimal size of 10–100 nm. In this size range, the particles are large enough to avoid kidney filtration and small enough to penetrate tissues. Furthermore, the delivery system can facilitate particles containing siRNA to enter cells via receptor-mediated endocytosis, promote intracellular trafficking, and minimize clearance mediated by reticuloendothelial system (RES); (3) the vector must be stable enough in physiological fluids to avoid nucleic acid degradation; (4) the vector should have the capability of escaping from opsonization and uptake by macrophages, maintaining high retention time, reaching, and entering the target cells; and (5) the escape of siRNA from the endosome and further release into the cytoplasm are also considered necessary.^{2,7,8} All of these properties are desired for the development of a powerful siRNA delivery system.

Many carriers have been developed to obtain ideal siRNA delivery, such as viral nanocarriers,⁹ lipid-based vectors,^{10–12} polymer-mediated nanoparticles,^{13–17} exosomes,^{18,19} and oligonucleotide nanoparticles.^{20,21} Among these carriers, a packaging RNA (pRNA)

Received 4 January 2017; accepted 19 June 2017;
<http://dx.doi.org/10.1016/j.omtn.2017.06.014>

⁴These authors contributed equally to this work.

Correspondence: Zhiping Li, Beijing Institute of Pharmacology and Toxicology, 27 Taiping Road, Haidian District, Beijing 100850, China.

E-mail: dearwood2010@126.com

nanoparticle is one of the most promising vectors due to its high potential in therapeutics and wide variety of functions.²² pRNA is a component of the bacteriophage phi29 DNA-packaging motor, its monomers can fold into stable and unique secondary structures to form dimers, trimers, and ultimately hexamers, which have optimal sizes ranging from 10–50 nm.^{23–26} The formation of polymerides is mediated through hand-in-hand interaction of the right and left interlocking loops.²³ This structural feature of pRNA allows for easy manipulation, high reproducibility, and known stoichiometry.²⁴ Fusion of pRNA with a variety of sequences at the specific sites do not impede the formation of polymerides or interfere with functions, which allows pRNA to carry therapeutic and targeting genes simultaneously without altering its secondary structure or intermolecular interactions.^{2,24} Another advantage of pRNA as a delivery system is its ability to avoid immune responses after long-term repeated drug administration.^{22–24,27,28} In all, pRNA nanotechnology provides a potential and innovative therapeutic strategy for treatment of gene-related diseases.⁸

Although promising in nucleic acid delivery, pRNA nanoparticles still face many hurdles in delivering siRNA. A major concern is its instability. pRNA nanoparticles are formed via non-covalent bonding, which results in thermodynamic instability and easy dissociation in vivo.^{26,27} Furthermore, a high concentration of magnesium ions of about 5 mM, which is much higher than the 0.35–0.70 mM in human blood, thus is usually required to maintain an appropriate pRNA conformation for all pRNA polymerides, including a stability-improved three-way junction-decorated hexamer.^{26,29} All of these problems should be solved to improve the delivery efficiency and therapeutic applications of pRNA nanoparticles.

Besides pRNA, chitosan is another candidate suitable for delivering genes because of its positive charge, good biocompatibility, favorable biodegradability, low cytotoxicity, and satisfactory chemical modification.^{2,30} Recently, the safety and efficient gene silencing of chitosan nanocarriers have been certified in vivo.³¹ However, the insufficient intracellular transport limits the wide application of chitosan carriers in siRNA delivery.³¹

Based on the above background, we first designed a dual tumor-targeting siRNA delivery system combining pRNA dimers with folate and polyethylene glycol (PEG)-decorated chitosan nanoparticles (CNPPs). The construction and proposed schematic illustration of CNPPs are shown in Figure 1. First, pRNA monomers with therapeutic siRNA (*c-Myc* siRNA) or a tumor-targeting aptamer (FB4, a RNA aptamer specifically binding to the extracellular domain of a transferrin receptor) were constructed by in vitro transcription, and after that, pRNA dimers simultaneously carrying therapeutic siRNA and a tumor-targeting aptamer were formed by mixing different pRNA monomers together. Then, chitosan nanocarriers loading pRNA dimers were developed by encapsulating pRNA dimers into folate and PEGylated chitosan nanoparticles using a modified ionic gelation method. After intravenous injection, chitosan nanoparticles act as the first class carrier of siRNA delivery to protect pRNA dimers from depolymerization, degradation, or elimination and deliver intact pRNA dimers near or

into target cells under the guidance of folate. pRNA dimers released outside the cells then play the role of the second class carrier of siRNA delivery and selectively enter target cells via receptor-mediated endocytosis or intercellular penetration facilitated by their small particle size. Accordingly, the significantly improved intracellular delivery and favorable therapeutic efficacy of siRNA was expected for this dual tumor-targeting siRNA delivery system since this system makes best use of the advantages of chitosan nanoparticles and pRNA dimers, while addressing their respective disadvantages.

To certify the practical siRNA delivering efficacy of this dual tumor-targeting nanocarrier system, CNPPs and other formulations of siRNA were constructed and their delivering efficiencies both in vitro and in vivo were evaluated in this study.

RESULTS AND DISCUSSION

Characterization of FA-PEG-Chitosan

Successful synthesis of folic acid (FA)-PEG-chitosan was confirmed by ¹H nuclear magnetic resonance (NMR) spectra, and the typical ¹H spectrum is shown in Figure 2. The degree of deacetylation (DD) of chitosan was speculated with signal A at $\delta = 1.8\text{--}1.9$ ppm from the acetyl group ($-\text{COCH}_3$), signal B at $\delta = 2.9\text{--}3.1$ ppm from the monosaccharide residue ($-\text{CH}(\text{OCH}) - (\text{CH})_2-$), and signal C at $\delta = 3.4\text{--}3.5$ ppm from PEG ($-\text{OCH}_2\text{CH}_2\text{O}-$), and the DD of chitosan was about 85%. The degree of substitution (DS) value of PEG on FA-PEG-chitosan was calculated according to the relative peak area of ethylene group of PEG (signal C) to monosaccharide residue (signal B), and it was about 25%. The relevant signals of folate are too weak compared with the broad and strong proton signals of PEG and chitosan residues to obtain the precise degree of folate grafting. Therefore, UV spectroscopy was used for accurate evaluation, and the DS of folate was 18%.

Characteristics In Vitro

pRNA dimers alone and the three derivatives of chitosan nanoparticles (i.e., chitosan nanoparticles containing siRNA with folate conjugation and PEGylation [CNPS], chitosan nanoparticles containing pRNA dimers only [CN], and chitosan nanoparticles containing pRNA dimers with folate conjugation and PEGylation [CNPPs]), were fabricated and characterized. pRNA dimers appeared regularly circular (Figures 3A–3C). All chitosan nanoparticles were round and there was no morphologic difference among these particles (Figures 3D–3L). The diameters of CNPS, CN, and CNPPs were 279.74 ± 1.63 nm, 321.54 ± 3.56 nm, and 352.57 ± 6.70 nm, respectively (shown in Figures 3M–3O), which was consistent between transmission electron microscopy (TEM) and atomic force microscopy (AFM) analyses. The diameters of CN and CNPPs were larger than CNPS, which was likely due to the larger volume of pRNA dimers compared to siRNA. The diameter of pRNA dimers was estimated between 20 nm and 30 nm (Figure 3A), since the concentration of pRNA dimers was too low to detect their diameters by photo correlation spectroscopy. The zeta potentials of pRNA dimers, CNPS, CN, and CNPPs were -27.4 ± 1.8 mV, 19.2 ± 1.3 mV, 21.5 ± 1.2 mV, and 16.7 ± 1.6 mV, respectively. The encapsulation efficiencies of CNPS, CN, and CNPPs were $64.3 \pm 1.2\%$, $65.8 \pm 2.3\%$, and $62.2 \pm 0.9\%$, respectively.

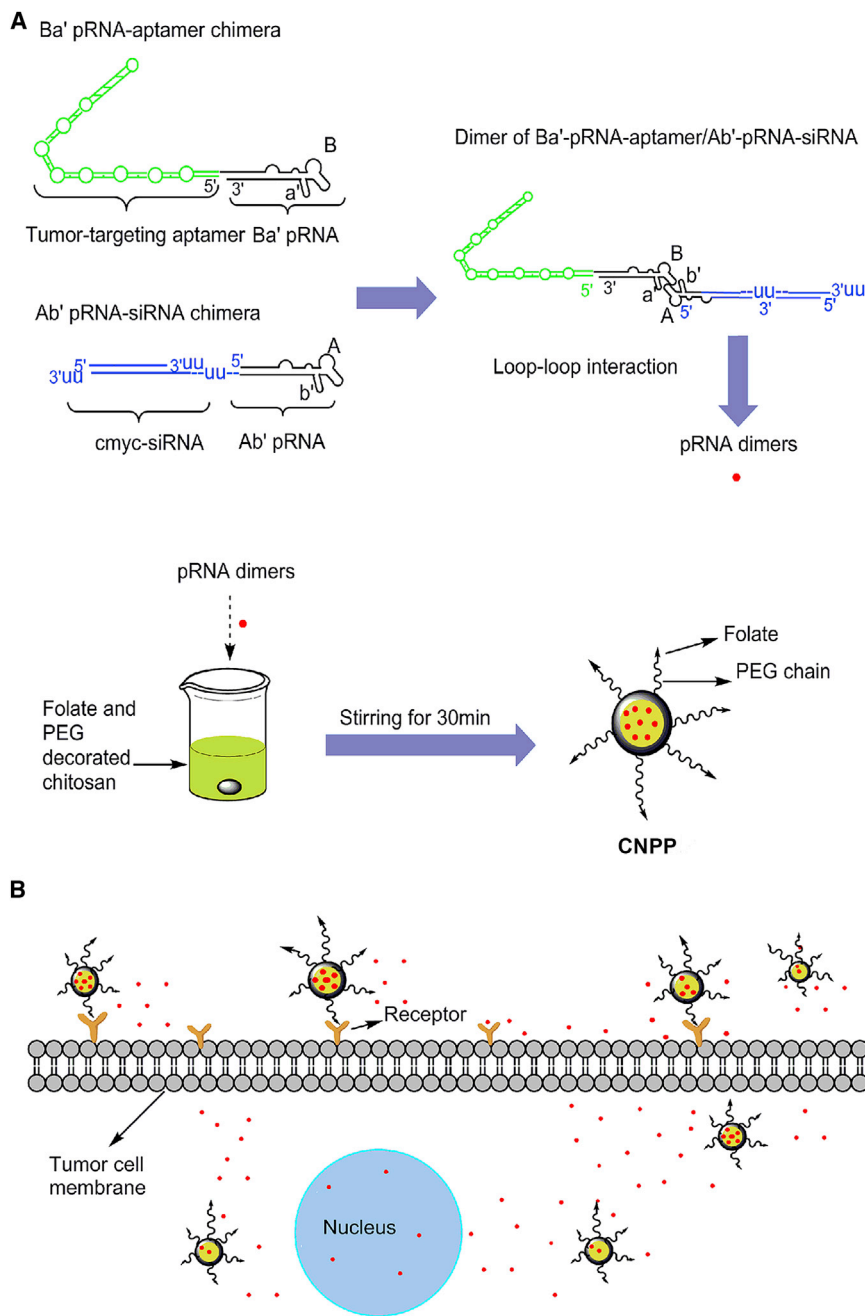


Figure 1. Preparation and Proposed Illustration of CNPPs

(A) Schematic of CNPPs preparation. First, pRNA monomer carrying tumor-targeting aptamer (Ba') and pRNA monomer carrying therapeutic siRNA (Ab') are constructed by in vitro transcription, and pRNA dimers simultaneously carrying therapeutic siRNA and tumor-targeting aptamers are formed spontaneously after the mixture of different pRNA monomers at a ratio of 1:1. Then, the formed pRNA dimer suspension containing sodium tripolyphosphate is added into the folate-conjugated and PEGylated chitosan solution. CNPPs are finally obtained after stirring for 30 min. (B) Proposed schematic illustration of designed CNPPs. After injection, chitosan nanoparticles in CNPPs act as the first class of dual delivery system to protect pRNA dimers from depolymerization, degradation, or elimination and deliver the intact pRNA dimers near or into target cells under the guidance of folate. pRNA dimers released outside the cells then play the role of the second class of dual delivery system and enter into the target cells via receptor-mediated endocytosis or intercellular penetration facilitating the advantage of small particle size.

lower drug loading and lower encapsulation efficiency. Therefore, CNPPs with diameters about 300 nm were applied in this study after overall consideration.

Colloidal Stability

The colloidal stability of CNPPs and their dilutions with 5% glucose solution, minimum essential medium (MEM) containing 10% fetal bovine serum (FBS) or mouse serum, was monitored by Turbiscan Lab Expert, as shown in Figure 4. The variations of each sample in transmission or backscattering profiles during 2 days were exhibited and less than 3% of variations in both transmission and backscattering for all samples were observed. These changes were considered negligible when it was below 3%, and we concluded that no apparent aggregation, depolymerization, or sedimentation occurred in any samples during culture. Therefore, CNPPs were deemed stable, and the stability of pRNA dimers encapsulated in CNPPs was also considered to be improved since the instability of pRNA dimers has been well characterized previously.^{7,26} Furthermore, CNPPs have also been shown to enhance the stability of siRNA both in vitro and in vivo.^{3,30}

It was previously reported that nanoparticle size affected the bio-distribution of nanoparticles and nanoparticles with diameters larger than 200 nm were prone to activate the complement system, be rapidly removed from the blood stream, and accumulate in the liver and spleen.³² However, PEGylation of nanoparticles, even >500 nm, allow their escape from the macrophage system and prolong their circulation.³³ In fact, CNPPs with diameters about 200 nm were also obtained in our experiments, and they were not used in further experiments since the lower particle size of CNPPs could lead to

Cellular Uptake and Confocal Microscopy Analysis

The intracellular uptake of free siRNA and different chitosan nanoparticle formulations was quantitatively evaluated by flow cytometry. As shown in Figure 5A, CNPPs had the strongest geometric mean

It was previously reported that nanoparticle size affected the bio-distribution of nanoparticles and nanoparticles with diameters larger than 200 nm were prone to activate the complement system, be rapidly removed from the blood stream, and accumulate in the liver and spleen.³² However, PEGylation of nanoparticles, even >500 nm, allow their escape from the macrophage system and prolong their circulation.³³ In fact, CNPPs with diameters about 200 nm were also obtained in our experiments, and they were not used in further experiments since the lower particle size of CNPPs could lead to

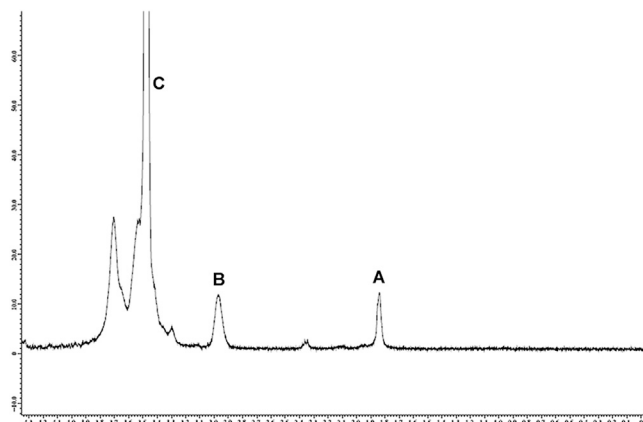


Figure 2. Verification of Synthesized FA-PEG-Chitosan

^1H NMR spectrum of FA-PEG-chitosan with 25% DS of PEG and 18% grafting degree of folate in D_2O containing two drops of 20% $\text{DCI}/\text{D}_2\text{O}$. (A) The signal from the acetyl group at $\delta = 1.8\text{--}1.9$ ppm. (B) The signal from the monosaccharide residue at $\delta = 2.9\text{--}3.1$ ppm. (C) The signal from PEG at $\delta = 3.4\text{--}3.5$ ppm.

intensity in MCF-7 cells, followed by pRNA dimers, CN, and CNPS, while free siRNA had the lowest cellular uptake. It was reasonable for free siRNA to show poor cell uptake, since cellular uptake is hindered due to its negative charge, large size, and instability.^{3,30} The cellular uptake of CNPS was minimal, which could be attributed to its large particle size, limited endocytosis mediated by ligand, and poor cell penetrating ability of free siRNA released from CNPS. The cellular uptake of pRNA dimers was significantly increased compared with CNPS, likely due to the targeting action of FB4, except the small particle size and factitiously improved stability by the culture medium without FBS, since FB4 has been shown to specifically bind the extracellular domain of transferrin receptors overexpressed by MCF-7 cells.³⁴ The cellular uptake of CN was higher than CNPS, while lower than pRNA dimers, primarily related to the partial release of pRNA dimers from CN, since CN did not readily enter cells because of its large size and absent endocytosis mediated by ligand. The highest cellular uptake of CNPPs was attributed to two reasons. First, PEGylation and folate conjugation on chitosan rendered CNPPs long circulation and high targeting ability, which could improve the entry of CNPPs into the target cells by endocytosis.^{30,31} Second, CNPPs could protect pRNA dimers from degradation and bring pRNA dimers near to the target cells, where pRNA dimers were released and easily entered the target cell utilizing FB4 and the proper size.^{7,23} The effect of binding action between a transferrin receptor and FB4 on cellular uptake was also evaluated by adding 50-fold free FB4 into the samples with different formulation before treatment. The results showed that the cellular uptake of pRNA was significantly inhibited for nanocarriers decorated with a FB4 aptamer when free FB4 was simultaneously added into the cell culture, while there was no difference in the cellular uptake of siRNA encapsulated in CNPS without the addition of FB4. Thereby, this data suggested that FB4 could bind with a transferrin receptor expressed by MCF-7 cells, and this binding could significantly improve the cellular uptake of siRNA.

The cell penetrating efficiency of free siRNA and different formulations was further evaluated by confocal laser scanning microscopy (CLSM), and the results are shown in Figure 5D. There was almost no green fluorescence in cells treated with free siRNA, the apparent green fluorescence was exhibited in cells treated with other samples and the strongest appeared in cells cultured with CNPPs. This result was in agreement with the outcome of cellular uptake by flow cytometry analysis, that is, the combination of targeting chitosan nanoparticles and pRNA dimers improved the cellular uptake of siRNA compared with targeting chitosan nanoparticles or pRNA dimers alone. The fluorescence intensity decreased in cells simultaneously treated with free FB4 and formulations decorated with FB4, while there was no apparent change in cells simultaneously treated with free FB4 and CNPS, which indicated that a free FB4 aptamer could competitively bind with a transferrin receptor expressed by MCF-7 cells.

Cell Apoptosis Assay

Apoptosis of MCF-7 cells was evaluated after transfection with various formulations, and the cells were analyzed after staining with Annexin V-fluorescein isothiocyanate (FITC) and propidium iodide (PI). As shown in Figure 5E, significant apoptosis (23%–43%) was exhibited in cells treated with different formulations containing siRNA, while minimal apoptosis was observed in control cells and cells treated with free siRNA or CNPPs with negative control siRNA (negative control), which indicated that the apoptosis response originated from the downregulation of *c-Myc* in MCF-7 cells.^{35,36} During the four different formulations encapsulating siRNA, the highest apoptosis of about 43% was seen in cells treated with CNPPs, the higher apoptosis of about 37% was observed in cells treated with pRNA dimers, and the lowest apoptosis of 23% was in cells treated with CNPS. This trend was consistent with that from cellular uptake and CLSM analysis, which illustrated the advantages of combining targeted CNPPs with pRNA dimers.

Cell Cytotoxicity

Toxicity of different particles was evaluated on MCF-7 cells using a 3-(4, 5-dimethylthiazol-2-yl)-2,5-diphenyltetrazolium bromide (MTT) reduction assay as shown in Figure 5B. The results depicted that the cell viability decreased over the culture time for all samples. Furthermore, there was almost no cytotoxicity shown for free siRNA, while obvious cytotoxicity was displayed for other formulations in which CNPPs exhibited the strongest cytotoxicity. The effects of CNPS and CN on MCF-7 cells were unsatisfactory, as it was higher than free siRNA. Compared with CNPS, the pRNA dimer showed significant cytotoxicity. The highest cytotoxicity was in CNPPs as expected, which confirmed that the significantly improved intracellular siRNA delivery was due to the comprehensive actions of pRNA dimers^{7,26} and targeting chitosan nanoparticles.³¹

In Vitro Gene Silencing

In vitro gene silencing was examined by the real-time qPCR analysis and results are shown in Figure 5C. There was no *c-Myc* suppression found in cells treated with negative control compared with the cells treated with blank culture media, while *c-Myc* expression was

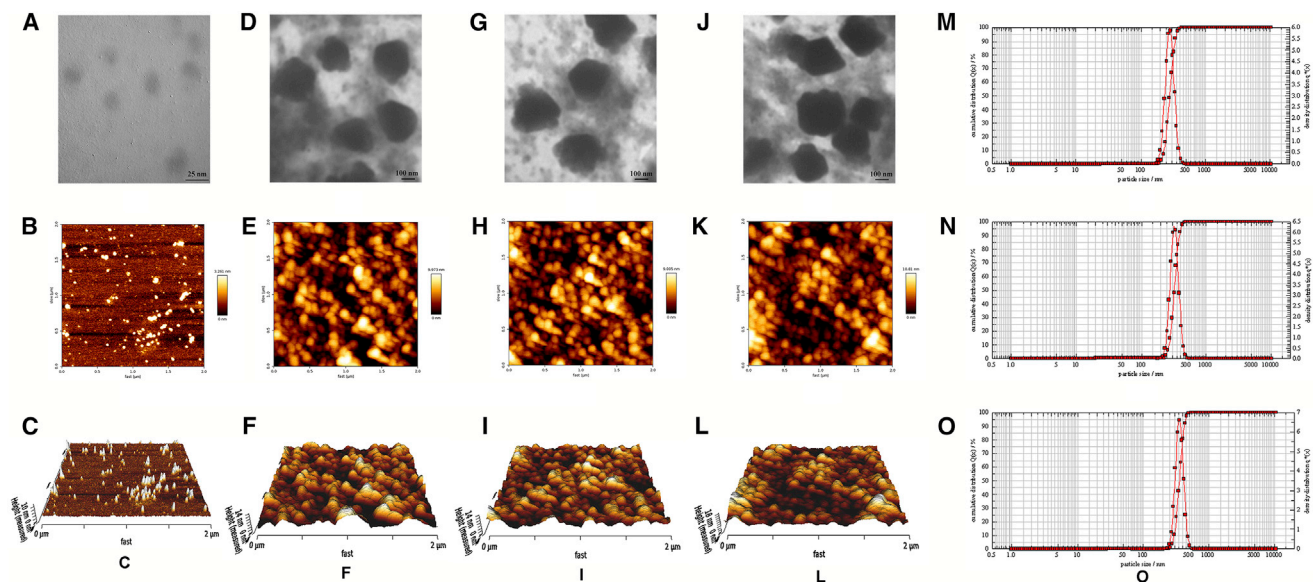


Figure 3. Characteristics of Various Nanoparticles

(A–C) Transmission electron microscopy image (A) and atomic force microscopy images (B, plane surface image; C, three-dimensional image) of pRNA dimers. (D–F and M) Transmission electron microscopy image (D), atomic force microscopy images (E, plane surface image; F, three-dimensional image), and particle size distribution (M) of CN. (G–I and N) Transmission electron microscopy image (G), atomic force microscopy images (H, plane surface image; I, three dimension image), and particle size distribution (N) of CNPs. (J–L and O) Transmission electron microscopy image (J), atomic force microscopy images (K, plane surface image; L, three dimension image), and particle size distribution (O) of CNPPs.

downregulated at different degrees in cells treated with different nanoparticle formulations carrying *c-Myc* siRNA, which suggested that no non-specific gene silencing occurred. The *c-Myc* expression was also hardly suppressed by free siRNA. In all formulations, CNPs showed the lowest *in vitro* gene silencing, which was perhaps related with the low membrane permeability due to its large size and limited cell endocytosis. While pRNA dimers may show higher gene silencing *in vitro* due to its ideal size, their increased sensitivity to RNases may render them impractical for *in vivo* silencing. CN exhibited moderate gene silencing ability between CNPs and pRNA dimers, which was perhaps related to the partially released pRNA dimers. CNPPs showed the highest mRNA inhibition, since it combined with the advantages of pRNA dimers and chitosan nanoparticles. These data were in agreement with the results from cellular uptake, CLSM, and cell apoptosis assay.

In Vivo Distribution of siRNA

To evaluate the tumor-targeting effects of the nanoparticles, the *in vivo* distribution and tumor accumulation of the cyanine 7 (Cy7)-siRNA or Cy7-pRNA dimer were visualized by monitoring the whole body fluorescence intensity with a NightOWL II *in vivo* imaging system. Cy7-labeled free siRNA, CN, CNPs, and CNPPs were injected into MCF-7 xenograft-bearing nude mice, and the results are shown in Figure 6A. pRNA dimers were not investigated since they were highly unstable *in vivo* due to the dissociation at ultra low concentration after systemic injection,²⁶ degradation by RNase,⁷ and complexation with proteins in serum.²⁷

Significantly different distribution of fluorescence signals was observed among mice administered the different nanoparticle formulations. No fluorescence signals were detected during the whole experimental period for the negative control mice treated with 5% glucose. The fluorescence distributed systematically soon after administration in mice administered free siRNA, accumulated gradually in the bladder, and disappeared completely at 24 hr after injection, and there was no siRNA accumulation at the tumor site. Similar to free siRNA, the systemic distribution of fluorescence was also found in mice treated with CN, CNPs, and CNPPs soon after injection. The signal of fluorescence seemed to attenuate more in mice treated with CN than mice treated with CNPs or CNPPs, which was likely due to PEGylation in CNPs and CNPPs formulations, thereby prolonging the circulating time.³⁰ The fluorescence in mice treated with CN completely disappeared except for the kidney at 24 hr, and there was no fluorescence found at the tumor site. The fluorescence in mice administered CNPs focused on the kidneys, and tumors gradually with time, and the strong fluorescence in the kidneys and the slight fluorescence in tumors were observed at 24 hr. This was perhaps reasonable since the bladder was an excretory organ, and a folate receptor was overexpressed in malignant cells.³¹ In contrast, obvious fluorescence appeared in tumors for mice administered CNPPs, which indicated the stronger and more specific targeting of CNPPs than either CN or CNPs to the tumor. This might be attributed to the combination of targeting chitosan nanoparticles and pRNA dimers.

Tissues and organs were harvested for observation at the end of the imaging period, and the results are shown in Figure 6B. No

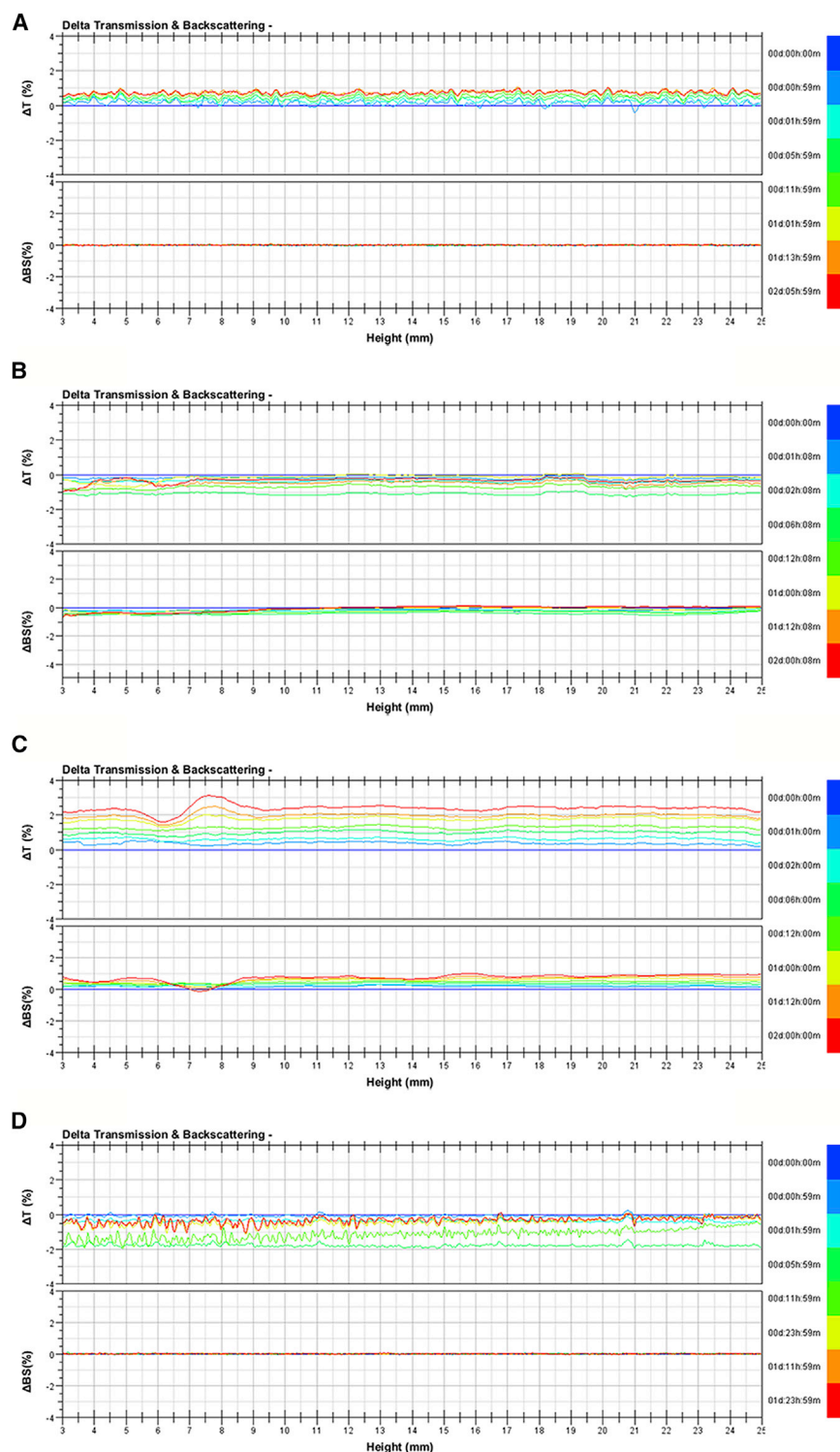


Figure 4. Colloidal Stability Analysis of CNPPs

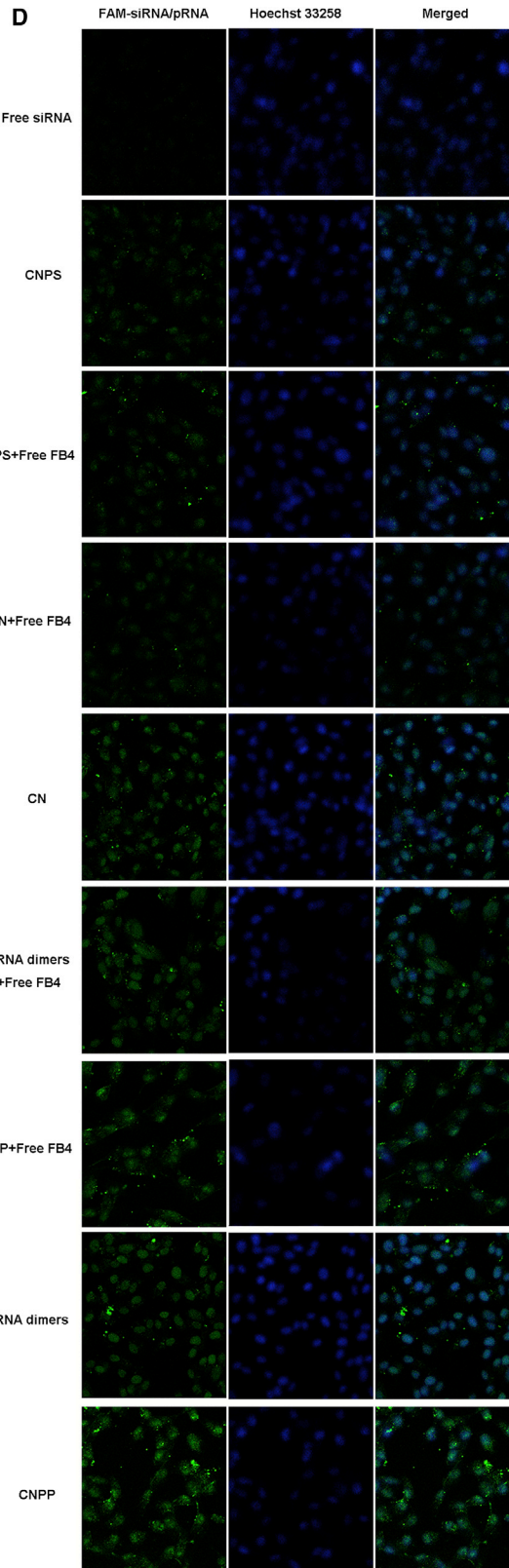
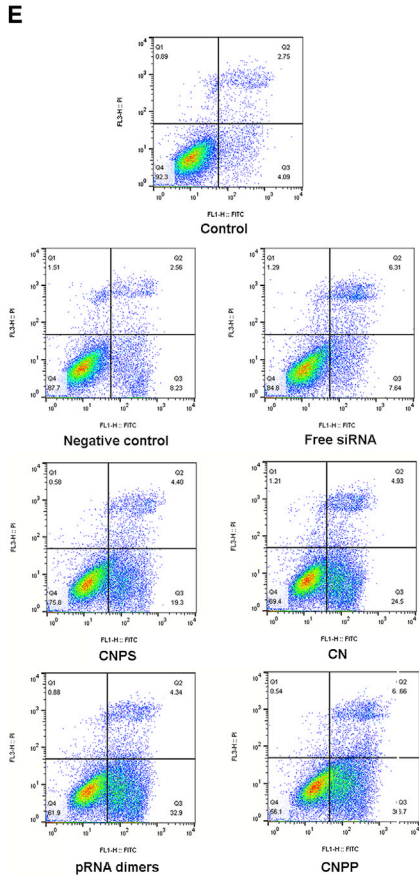
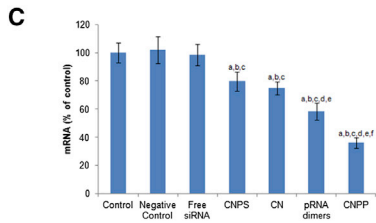
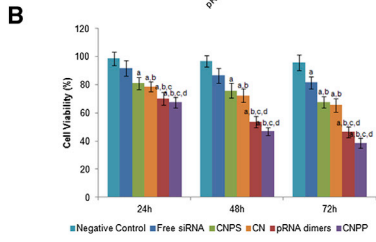
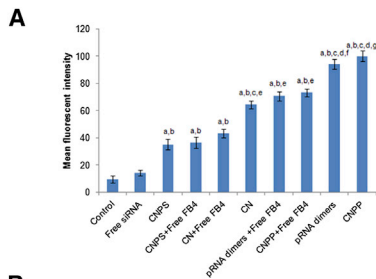
(A) Variation profiles of transmission and backscattering for CNPPs at 37°C. (B) Variation profiles of transmission and backscattering for CNPPs diluted 50-fold with 5% glucose solution at 37°C. (C) Variation profiles of transmission and backscattering for CNPPs diluted 50-fold with MEM culture media containing 10% FBS at 37°C. (D) Variation profiles of transmission and backscattering for CNPPs diluted 50-fold with mouse serum at 37°C. All of these experiments were performed in triplicate.

administered CN was mainly distributed in the liver, spleen, and kidney, and there was slight and negligible fluorescence observed in the heart and tumor. This was perhaps related to the phagocytosis of nanoparticles caused by the reticuloendothelial system, since these particles were not conjugated with a folate or PEG. The distribution of fluorescence in mice administered CNPs and CNPPs was similar and the fluorescence majorly localized in the kidney and tumor, while small amounts were observed in the liver and spleen. Although the fluorescence distribution in mice between CNPs and CNPPs was similar, significantly higher fluorescence was observed in the tumor in mice administered CNPPs than CNPs. The similarity of fluorescence distribution in mice for CNPs and CNPPs was perhaps related to their similar particle size and PEGylation and folate conjugation, and the difference in the amount of fluorescence in the tumor was considered caused by the difference between free siRNA and pRNA dimers since released pRNA dimers with FB4 could specifically bind with a transferring receptor secreted by MCF-7 tumor cells and enter into the tumor cells by endocytosis or due to their small size, while free siRNA released from chitosan nanoparticles was rapidly eliminated because of its extreme instability *in vivo*.

The nude mouse, a laboratory mouse from a strain with a genetic mutation that causes a deteriorated or absent thymus and thereby an inhibited immune system due to a greatly reduced number of T cells, was selected as the animal model for *in vivo* experiments in this study. *Nu/Nu* mice can receive various tissue and tumor grafts, as they mount no rejection response. It is worth noting that the *nu/nu* mouse has normal B cells, natural killer (NK) cells, macrophages, and granulocytes. Therefore, the nude mouse is widely used for *in vivo* evaluation of antitumor drugs encapsulated in nanoparticles.^{19,35,36}

fluorescence was detected in any tissue or organ for mice in the negative control group and mice administered free siRNA, likely due to the rapid *in vivo* clearance for free siRNA. The fluorescence in mice

mouse has normal B cells, natural killer (NK) cells, macrophages, and granulocytes. Therefore, the nude mouse is widely used for *in vivo* evaluation of antitumor drugs encapsulated in nanoparticles.^{19,35,36}



(legend on next page)

The process of *in vivo* uptake of these nanoparticles might be speculated as follows. First, both CNPPs and CNPS were distributed generally soon after administration and then selectively combined with the cells expressing the folate receptor, such as cells in a tumor and activated macrophages. Then, some of the siRNA in CNPS entered the above cells by folate-mediated endocytosis, the rest were released from CNPS and degraded gradually because of the poor permeability and stability of siRNA. Similarly, some of the pRNA dimers in CNPPs also entered the cells expressing a folate receptor, and the rest were isolated from nanoparticles. However, the difference was that pRNA dimers carried both siRNA and aptamers and could remain intact *in vivo* under the protection of chitosan nanoparticles, thereby, both the endocytosis mediated by the specific aptamer and the cell membrane permeability caused by the satisfactory particle size could significantly improve the distribution of siRNA in a tumor. Therefore, CNPPs integrated the advantages of both targeting chitosan nanoparticles and pRNA dimers and showed notable improvement in siRNA delivery efficacy.

In Vivo Antitumor Efficiency

The antitumor efficacy of different formulations was further investigated in MCF-7 tumor-bearing mice following the *in vitro* studies. As shown in Figure 7A, the tumor volume of mice administered both 5% glucose and free siRNA increased with time and there was no statistical difference in tumor growth, which indicated that free siRNA exhibited no antitumor efficacy *in vivo*. Tumor inhibition was observed to different degrees in mice receiving various formulations encapsulating siRNA, and the order of antitumor efficiency was CNPPs > CNPS > CN, which was concordant with the results from an *in vivo* distribution experiment. Contrary to the results *in vitro*, CN displayed weaker tumor inhibition than CNPS, which was related directly to the absence of tumor targeting for CN and poor stability of pRNA dimers. The body weight variations over the treatment period were also monitored to estimate the toxic side effects of various formulations. As shown in Figure 7B, there was no apparent reduction in body weight of the mice treated with various nanoparticle formulations. No obvious changes in spirits were observed for these mice. Therefore, it could be supposed that these nanoparticle formulations were safe.

Pharmacokinetic and Biodistribution Study

To verify the prolonged circulating time of PEGylated particles, pharmacokinetic analysis of siRNA in different formulations was performed in mice, and the results are shown in Figure 7C. It was obvious

that naked siRNA was cleared at the fastest speed and almost completely eliminated at 120 min post-injection. After encapsulating with common chitosan nanoparticles, the clearance of siRNA slightly slows down, which means that chitosan nanoparticles protect siRNA from elimination to some extent. Compared with CN, the plasma concentration of siRNA in folate-conjugated and PEGylated chitosan nanoparticles (both CNPS and CNPPs) displayed a slower elimination rate and sustained for a longer time. This suggested that functionalization of nanoparticles with PEG moieties prolonged the circulating time in blood. However, it's worth noting that the detected object was the fluorescence intensity of Cy7 rather than siRNA or pRNA itself, that is, the results were not influenced if siRNA or pRNA was degraded while Cy7 was still intact. Therefore, the method used to detect siRNA or pRNA here was not accurate enough, and the result acquired by this method was just reference.

To further explain the therapeutic efficacy disparity of siRNA with different formulations, the biodistribution of siRNA in mice was investigated and the results are displayed in Figure 7D. It was obvious that the strongest fluorescence was shown in the liver and most of the fluorescence mainly accumulated in the liver, kidney, lung, and spleen at 1 hr for all mice in spite of formulation. The fluorescence quickly disappeared in almost all tissues at 8 hr except the kidney for naked siRNA, and it could be detected in the liver, spleen, and kidney until 24 hr for CN, CNPS, and CNPPs. The strongest fluorescence in the MCF-7 tumor was detected in mice given CNPPs, the next appeared in mice given CNPS, and both were stronger than that in mice given CN. The fluorescence accumulation in the HT-1080 tumor was significantly decreased compared with that in the MCF-7 tumor for both CNPS and CNPPs, which resulted in that there was no significant difference in the fluorescence accumulation in the HT-1080 tumor for CN, CNPS, and CNPPs. Different from the tumor accumulation of CNPS and CNPPs, there were no changes found in fluorescence distribution between mice bearing a MCF-7 tumor and a HT-1080 tumor for both naked siRNA and CN. All of these data suggested that FA-decorated particles could selectively target to a transferrin-receptor positive MCF-7 tumor and CNPPs, the dual tumor-targeting nanocarrier system, which possessed a stronger targeting ability to a MCF-7 tumor than others.

Conclusions

A dual tumor-targeting nanocarrier system combining pRNA dimers and tumor-targeting chitosan nanoparticles for siRNA delivery was successfully developed in this study. The constructed system

Figure 5. Cellular Evaluation of Various Formulations

(A) Cellular uptake of various formulations into MCF-7 cells. a, $p < 0.05$ versus control; b, $p < 0.05$ versus free siRNA; c, $p < 0.05$ versus CNPS; d, $p < 0.05$ versus CN; e, $p < 0.05$ versus CN + free FB4; f, $p < 0.05$ versus pRNA dimers + free FB4; and g, $p < 0.05$ versus CNPPs + free FB4. This experiment was performed in triplicate. (B) Cytotoxicity of different formulations against MCF-7 cells at different times. a, $p < 0.05$ versus negative control; b, $p < 0.05$ versus free siRNA; c, $p < 0.05$ versus CNPS; and d, $p < 0.05$ versus CN. This experiment was repeated six times. (C) Level of *c-Myc* mRNA determined by real-time qPCR. a, $p < 0.05$ versus control; b, $p < 0.05$ versus negative control; c, $p < 0.05$ versus free siRNA; d, $p < 0.05$ versus CNPS; e, $p < 0.05$ versus CN; and f, $p < 0.05$ versus pRNA dimers. This experiment was performed in triplicate. (D) CLSM analysis for the uptake of various formulations by MCF-7 cells. Hoechst 33258 for nuclei staining (blue) and FAM-siRNA/FAM-pRNA dimer fluorescence (green) were recorded. This experiment was performed in triplicate. (E) Induction of cell apoptosis by different formulations. Early apoptotic cells are presented in the lower right quadrant, late apoptotic cells are presented in the upper right quadrant, necrotic cells are presented in the upper left quadrant, and healthy cells are represented in the lower left quadrant. This experiment was performed in triplicate. The data in (A)–(C) represent mean and SD.

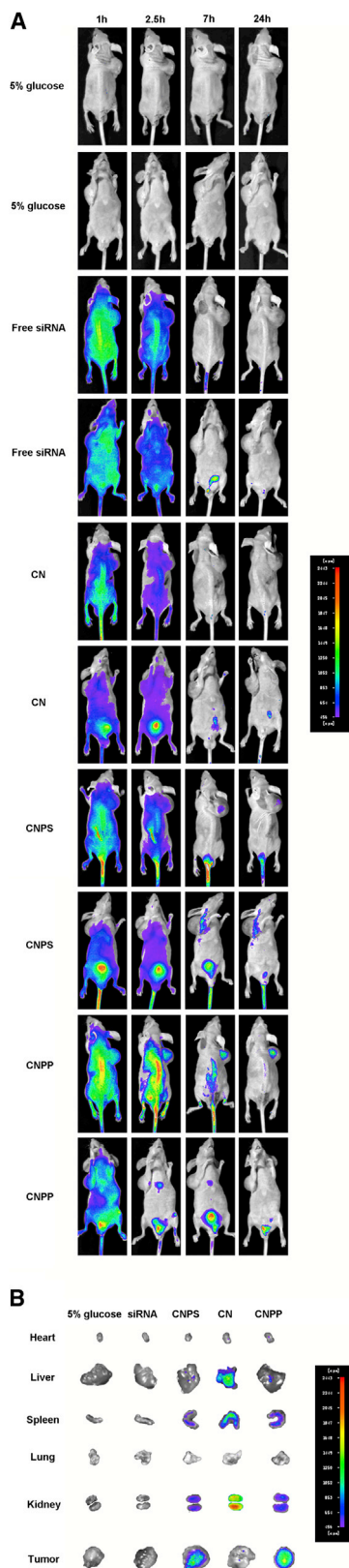


Figure 6. Imaging of Mice Bearing MCF-7 Tumor Xenografts

(A) The whole body imaging of mice bearing MCF-7 tumor xenografts at 1 hr, 2.5 hr, 4 hr, and 7 hr after intravenous injection of 5% glucose, Cy7-labeled siRNA, Cy7-labeled CN, Cy7-labeled CNPS, and Cy7-labeled CNPPs. (B) The isolated main tissue and organ imaging of mice bearing MCF-7 tumor xenografts at 24 hr after intravenous injection of 5% glucose, Cy7-labeled siRNA, Cy7-labeled CN, Cy7-labeled CNPS, and Cy7-labeled CNPPs. Both experiments were performed in triplicate.

displayed good physicochemical properties such as proper particle size, satisfactory encapsulation efficiency, and good colloidal stability. Importantly, this dual tumor-targeting nanocarrier exhibited the advantages and bypassed the disadvantages of pRNA dimers and chitosan nanoparticles and showed stronger tumor inhibition both in vitro and in vivo than pRNA dimers or tumor-targeting chitosan nanoparticles alone. Therefore, this system shows a number of superior features and is promising as a new generation of siRNA delivery systems. This dual tumor-targeting nanocarrier system may be valuable in future studies that utilize a pRNA hexamer, since it can simultaneously carry at most six different substances including therapeutic siRNA and ligands and can also be encapsulated into CNPPs by substituting pRNA dimers.

MATERIALS AND METHODS

Materials

Chitosan (molecular weight: 50 kDa and DD: 85%) was purchased from Nantong Xingcheng Biological Industrial Limited. FA, dicyclohexylcarbodiimide (DCC), N-hydroxysuccinimide (NHS), and 2-aminoethanethiol (AET) were obtained from Sinopharm Chemical Reagent. NHS-PEG-maleimide (NHS-PEG-MAL; molecular weight: 3,400 Da) was purchased from Shanghai Yare Biotech. Lyophilized *c-Myc* siRNA against *c-Myc* mRNA (5'-AACGUUAGCUUCACCAACAUTT-3'), negative control siRNA (siN.C., 5'-ACGUGACACGUUCGGAGAA TT-3'), carboxyfluorescein-labeled siRNA (FAM-siRNA), and Cy7-labeled siRNA (Cy7-siRNA) were purchased from GenePharma. Hoechst 33258 and MTT were purchased from Sigma-Aldrich. All chemicals were of reagent grade and obtained from Sinopharm Chemical Reagent unless stated otherwise.

MCF-7 cells and HT-1080 cells were purchased from the Cell Resource Centre (Institute of Biology and Medical Sciences, Chinese Academy of Medical Sciences & Peking Union Medical College). Male *nu/nu* nude mice (weighing 18–20 g) were purchased from Vital River Laboratories. Mice were all housed in ventilated cages with free access to food and water under standardized conditions. Mice were acclimatized to laboratory conditions for 7 days before experiments. At the same time, a dim red light was used for mice treated during the dark phase. All surgeries were performed under sodium pentobarbital anesthesia and all efforts were made to relieve suffering. All animals were handled in research according to the code of ethics defined by the Animal Care and Use Ethics Committee of Academy of Military Medical Sciences.

Synthesis and Purification of FA-Conjugated and PEGylated Chitosan

FA-PEG-chitosan was synthesized according to published literature.^{37,38} The synthesis was fulfilled through three steps, that is, the

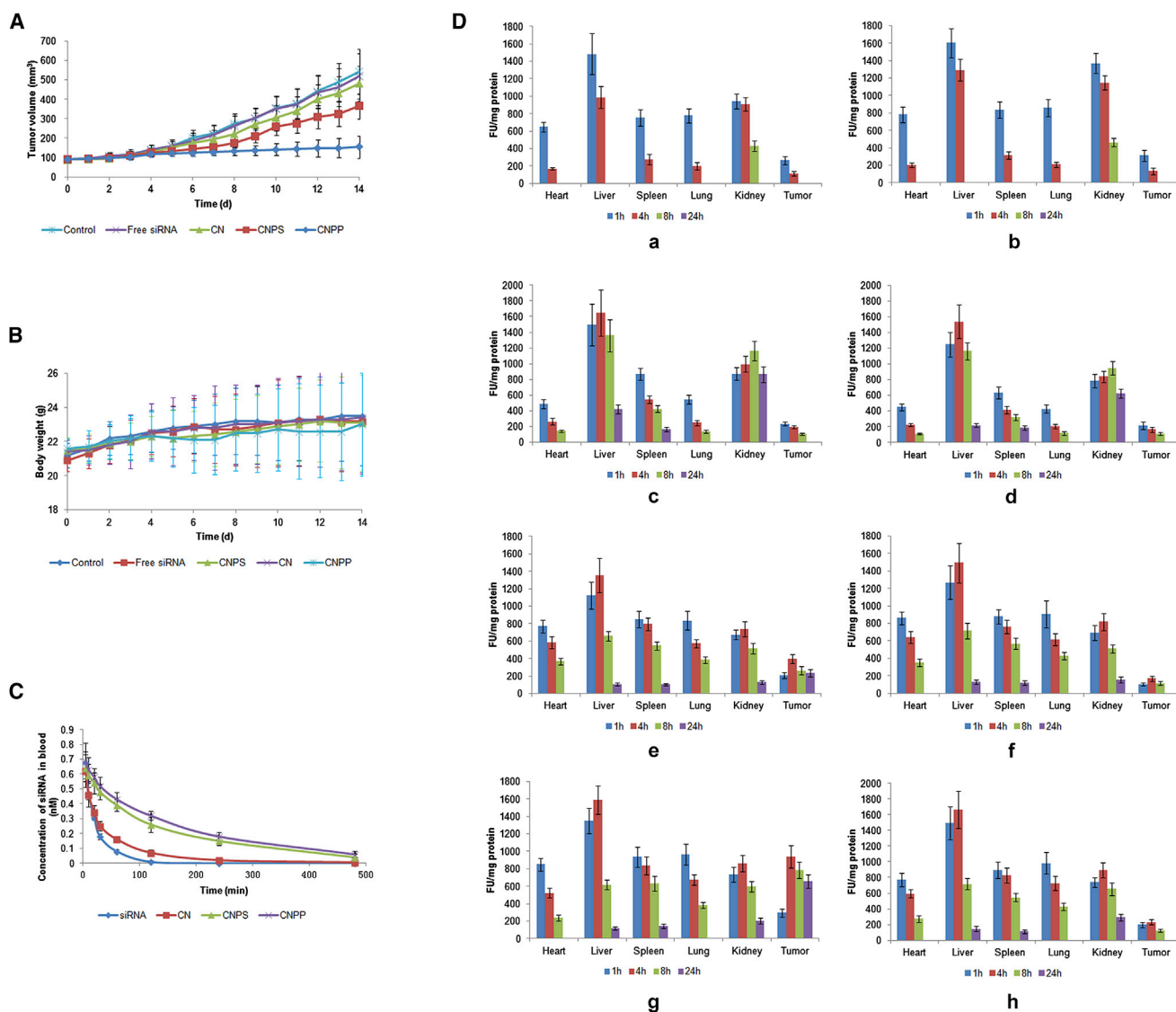


Figure 7. Pharmacodynamic, Pharmacokinetic, and Biodistribution Study of Various Formulations in Mice

(A) Tumor volume changes in MCF-7 tumor-bearing mice after treatment with 5% glucose and siRNA/pRNA encapsulated in various formulations. This experiment was repeated five times. (B) Body weight changes in MCF-7 tumor-bearing mice after treatment with 5% glucose and siRNA/pRNA encapsulated in various formulations. This experiment was performed five times. (C) Plasma concentration-time profiles of siRNA in mice after intravenous administration of Cy7-labeled siRNA, Cy7-labeled CN, Cy7-labeled CNPS, and Cy7-labeled CNPPs, respectively, via tail vein injection at the siRNA dose of 0.125 mg/kg. This experiment was performed in triplicate five times. (D) Fluorescence level attained in different tissues of mice bearing MCF-7 tumor (a, c, e, and g) or HT-1080 tumor (b, d, f, and h) at 1 hr, 4 hr, 8 hr, and 24 hr after intravenous administration of Cy7-labeled siRNA (a and b), Cy7-labeled CN (c and d), Cy7-labeled CNPS (e and f), and Cy7-labeled CNPPs (g and h). This experiment was performed in triplicate and all data represent mean and SD.

synthesis of NHS-conjugated FA (FA-NHS), the synthesis of thiol-conjugated FA (FA-SH), and the synthesis of FA-PEG-chitosan. First, FA (1.0 g) was added into the mixture of anhydrous DMSO (40 mL) and triethylamine (TEA, 0.5 mL) under stirring. The obtained solution was then mixed with DCC (0.5 g) and NHS (0.52 g) and stirred in the dark overnight. The production was filtrated to remove precipitation and FA-NHS was acquired after the filtrate was evaporated under vacuum. Second, FA-NHS was dissolved into the mixture of

DMSO and TEA (2:1, v/v), and then AET was added into the above mixtures to conduct the reaction. After overnight, the thiol group was linked to FA and FA-SH was obtained. Third, about 100 mg of deacetylated chitosan was dissolved in 20% acetic acid solution, and then the solution was adjusted to pH 6. The solution was further adjusted to pH 7 after the addition of about 100 mg NHS-PEG-MAL, and thereafter the reaction was performed under an argon atmosphere. After overnight reaction, PEGylated chitosan was acquired.

FA-SH was then slowly added to PEGylated chitosan solution under stirring, and the reaction was maintained for 48 hr after the mixture was adjusted to pH 6.5–7.5 with 6 M sodium hydroxide. After dialysis and following freeze drying, FA-PEG-chitosan was finally obtained in yellow powder and verified by ^1H NMR spectroscopy. Folate content of the final product was determined by a UV/V is spectrophotometer using the molar extinction coefficient value of $6,197 \text{ mole}^{-1} \text{ cm}^{-1}$ at $\lambda = 363 \text{ nm}$.³⁷

Generation of Chimera RNAs and Fluorescent RNAs

Regular pRNA-aptamer chimera and pRNA-siRNA chimera were generated by in vitro T7 transcription as reported in recent literature.^{17,18,31} In brief, transcriptions were conducted in a mixture of $0.1 \mu\text{M}$ DNA template, 0.75 mM of each nucleoside triphosphate (NTP), $0.375 \text{ U}/\mu\text{L}$ T7 RNA polymerase, 40 mM tris (hydroxymethyl) aminomethane hydrochloride (Tris-HCl, pH 7.5), 15 mM magnesium chloride (MgCl_2), 5 mM DTT, 2 mM spermidine, and 0.01% (v/v) Triton X-100. The transcription products were obtained after incubation for 3 hr at 37°C , precipitation by ethanol, and finally purification with denaturing gels. RNAs including pRNA-aptamer chimera and pRNA-siRNA chimera were both transcribed with DuraScribe T7 Transcription Kit (EPICENTRE Biotechnologies) in vitro.^{23,28}

The full sequence of pRNA-FB4 chimera (Ab') is $5'$ -GUUGAUUGC GUGUCAUAUGCGGACGGGAUUGCGGCCGUUGUCUGUG GCGUCCGUUCGUCAUGUGUAUGUUGGGGAUAGGACGCU GAUUGAGUUCAGCCCACAUAC- $3'$, in which the underlined sequence is the binding sequence of FB4. pRNA-siRNA represents pRNA chimera (pRNA Ba') that harbors the sequences of *c-Myc* siRNA: $5'$ -AGAACGUUAGCUUCACCAACAUGUCAUG UGUAUGUUGGGGAUUAACGCCUGAUUGAGUUCGACCCAC AUACUUUGUUGAUUGUCCGUCAAUCAUGGUGUUGGUGAA GCUAACGUUCUUU- $3'$, in which the underlined sequences are the sequences of *c-Myc* siRNA. pRNA-negative control siRNA represents pRNA chimera (pRNA Ba') that harbors the sequences of negative control siRNA: $5'$ -AGUUCUCCGAACGUGUCACGUUUGUCAU GUGUAUGUUGGGGAUUAACGCCUGAUUGAGUUCGACCCA CAUACUUUGUUGAUUGUCCGUCAAUCAUGGACGUGACAC GUUCGAGAACUUU- $3'$, in which the underlined sequences are the sequences of negative control siRNA.

The chimeras were labeled with fluorescence by using the Silencer siRNA Labeling Kit as previously described.²³ FAM and Cy7-labeled chimera sense strands were prepared in this study.

Preparation of pRNA Dimers

To form the dimer of pRNA, Ba' pRNA-aptamer chimeras and Ab' pRNA-siRNA chimeras were mixed at a 1:1 molar ratio in the presence of 5 mM Mg^{2+} and 40 U RNase inhibitor as reported.^{23,39,40}

Preparation of Chitosan Nanoparticles

CNPPs, the dual tumor-targeting nanocarrier system, were prepared based on the modified ionic gelation method as previously described.^{2,41,42} First, about 100 mg FA-PEG-chitosan was dissolved

in 20 mL of 1% acetic acid after stirring and sonication. The solution was adjusted to pH 5.5 with 0.25 M sodium hydroxide, and proper MgCl_2 was further added into the above solution to maintain the concentration of Mg^{2+} at 5 mM . Then, sodium triphosphate pentabasic (TPP) solution ($10 \text{ mg}/\text{mL}$) containing 5 mM MgCl_2 was mixed with pRNA dimers. The nanoparticles were spontaneously formed upon mixing the above solutions with the ratio of 5:1 (chitosan to TPP, w/w) under constant magnetic stirring and then incubated for at least 30 min. The nanoparticles were finally dialyzed with molecular weight cut off (MWCO) of 300 kD (Spectra/Por, Spectrum Labs) against diethyl pyrocarbonate water for 24 hr.

CN, CNPS, and negative control were also prepared according to the preparing method of CNPPs.

In Vitro Characterization of pRNA Dimers and Chitosan Nanoparticles

Morphology

pRNA dimers and different chitosan nanoparticles were all morphologically characterized first by TEM. The suspension of pRNA dimers and dilutions of chitosan nanoparticles were dropped, respectively, on a copper grid to form a dry film at room temperature. Then the samples were negatively stained with 2% phosphotungstic acid, air-dried at room temperature once again, and observed using TEM.

The morphologies of pRNA dimers and chitosan nanoparticles were also observed by AFM. The pRNA dimers and dilutions of chitosan nanoparticles were spread onto a mica sheet, dried at room temperature, and observed with AFM.

Particle Size Analysis

The particle sizes of CNPPs, CN, and CNPS were determined by photo correlation spectroscopy (Nanophox) at 25°C , while the concentration of pRNA dimer was too low to detect. The measurements were performed in triplicate, and the results were reported as the mean value of 50% particle distribution.

Zeta Potential Measurements

Zeta potentials of pRNA dimers, CNPS, CN, and CNPPs were measured in triplicate with Malvern Zetasizer Nano ZS90 instrument (Malvern Instruments). CNPS, CN, and CNPPs were suitably diluted with RNase-free water before determination, and the results were all reported as the mean \pm SD.

Determination of Encapsulation Efficiency

The encapsulation efficiencies of CNPPs, CN, and CNPs were obtained from the determination of free pRNA dimers or siRNA.^{35,41} Briefly, the suspension of FAM-labeled CNPS, FAM-labeled CN, or FAM-labeled CNPPs was centrifuged at a high speed of $15,000 \times g$ for 30 min at 4°C to precipitate the nanoparticles, and the supernatant was then carefully collected. The contents of pRNA dimers and siRNA added or in supernatant were then determined using the spectrofluorometer. The entrapment efficiency was obtained according to Equation 1, where $W_{\text{total drug}}$ indicates the total amount of pRNA

dimers or siRNA added and $W_{\text{free drug}}$ indicates the amount of pRNA dimers or siRNA non-encapsulated in the supernatant.

$$\text{Encapsulation efficiency}(\%) = \frac{[W_{\text{total drug}} - W_{\text{free drug}}]}{W_{\text{total drug}}} \times 100\%$$

(Equation 1)

Colloidal Stability Analysis

To evaluate colloidal stability, CNPPs and their dilutions with 5% glucose solution, MEM containing 10% FBS, and mouse serum, were monitored, respectively, with Turbiscan Lab Expert (Formulation) at 37°C to determine the small changes of colloidal systems with delta transmission and delta backscattering as indexes.⁴³

In Vitro Cellular Uptake

To analyze the cellular uptake in vitro, MCF-7 cells were seeded in 6-well plates at a density of 2×10^5 cells/well. After 24 hr, the cells were washed with cool PBS and then incubated for 4 hr with different FAM-labeled samples including free siRNA, CNPS, pRNA dimers, CN, and CNPPs at a siRNA concentration of 75 nM. After triplicate washing with cool PBS, the cells were detached with 0.25% trypsin solution and further washed with cold PBS. The cellular uptake was measured with flow cytometry after the cells were resuspended in 0.3 mL PBS. The autofluorescence of the cells was used as control.^{44,45} To further clarify the binding ability of FB4 with a transferrin receptor, 50-fold free full-length FB4 was added into the samples containing CNPS, CN, pRNA dimers, or CNPPs before treatment as a transferrin receptor negative control.^{46–49}

Confocal Imaging

For CLSM analysis, MCF-7 cells were seeded at a density of 2×10^5 cells/well on a petri dish and cultured for 24 hr. The media were then exchanged with 2 mL of FAM-labeled samples including free siRNA, pRNA dimers, CN, CNPS, and CNPPs, respectively. The final concentration of a FAM-siRNA/FAM-pRNA dimer for each sample was 200 nM. After incubation for 4 hr, the media were removed and discarded. Thereafter, the cells were washed for three times and fixed with 4% paraformaldehyde for 20 min. Then the cell nuclei were stained by Hoechst 33258 for 10 min at an ambient temperature. Finally, the fluorescent images were analyzed using CLSM (UltraVIEW VoX, PerkinElmer).^{35,50} To further estimate the binding ability of FB4 with a transferrin receptor, the fluorescent images of MCF-7 cells treated with 50-fold free full-length FB4 and different formulations together were also analyzed.

Cell Cytotoxicity

To evaluate the in vitro cell cytotoxicities of different formulations, MCF-7 cells were seeded in 96-well plates and incubated for 24 hr. After washing with cool PBS, the cells were further incubated with 200 μ L different samples including blank culture media, free siRNA, negative control, pRNA dimers, CN, CNPS, and CNPPs at a siRNA concentration of 200 nM for another 24 hr, 48 hr, and 72 hr, respectively. Then, 20 μ L of MTT solution (5.0 mg/mL) was added into each

well, and the plates were incubated for 4 hr. The media was then removed and 200 μ L of DMSO was added to dissolve the formazan crystals. The absorbance of the solutions at 570 nm was measured with a 96-well plate reader (Model 680, Bio-Rad). The cell culture medium was used as a negative control (cell viability defined as 100%).^{45,51,52}

In Vitro Gene Silencing

MCF-7 cells were seeded in a 35-mm dish 1 day before transfection. To carry out the treatment, the cells were washed and then incubated further with different samples including blank culture media, free siRNA, negative control, CNPS, pRNA dimers, CN, and CNPPs at a siRNA concentration of 100 nM for 4 hr. After that, the cells were washed again with cold PBS and incubated further for 48 hr (for mRNA assays). The transfected cells were then collected. Then, *c-Myc* mRNA was evaluated with real-time qPCR.

The method for the real-time qPCR assay has been reported in the literature,³⁶ and the mRNA was assayed in this study with minor modifications. In brief, the analysis was carried out on the IQ5 Real-Time PCR Detection System (Bio-Rad), and the relative gene expression was quantified by the $2^{-\Delta\Delta C_t}$ method using the IQ5 Optical System Software version 2.0 (Bio-Rad). The primers for PCR amplification were as follows: glyceraldehyde 3-phosphate dehydrogenase (GAPDH) forward: 5'-GGGTGTGAACCATGAGAAGT-3'; GAPDH reverse: 5'-GACTGTGGTCATGAGTCCT-3'; *c-Myc* forward: 5'-GGCTAT TCTGCCCATTTGGGGAC-3'; and *c-Myc* reverse: 5'-GGCAGCA GCTCGAATTTCTTC-3'. Reaction parameters were: 95°C for 10 s, then 61°C for 30 s, 40 cycles. Specificity was verified by melt curve analysis and agarose gel electrophoresis.

Cell Apoptosis Assay

To assay cell apoptosis induced by different formulations, MCF-7 cells were cultured in 6-well plates and incubated until 50% confluence. The cells were then cultured with different samples including blank culture media, negative control, free siRNA, CNPS, pRNA dimers, CN, and CNPPs at a final siRNA concentration of 75 nM for 4 hr, and thereafter the media were changed to the fresh culture media. After 72 hr, cells were trypsinized, collected, and washed with cool PBS. The apoptotic cells were detected by flow cytometer using the Annexin V-FITC Apoptosis Detection Kit (BD Biosciences). The results were analyzed using FlowJo software (Tree Star).³⁵

In Vivo Imaging

The in vivo imaging was evaluated in MCF-7 tumor-bearing male nude mice. Briefly, the mice were subcutaneously injected in right axilla with 3×10^6 MCF-7 cells. The tumors were allowed to grow to a volume of approximately 300 mm³, and the mice were randomly divided into five groups. Each group of mice was administered with 5% glucose, free Cy7-siRNA, Cy7-labeled CNPS, Cy7-labeled CN, or Cy7-labeled CNPPs at a dose of 0.5 mg/kg converting to siRNA by tail vein injection. Subsequently, the fluorescence imaging was performed with a NightOWL II in vivo Imaging System (LB983, Berthold Technologies) at a predetermined time.^{36,53} The mice were

then sacrificed by cervical dislocation after whole body imaging. The tumors and major organs including the heart, liver, spleen, lung, and kidney were finally excised and imaged.

In Vivo Antitumor Efficacy

The xenograft tumor model was established on male nude mice by subcutaneous injection of MCF-7 cells. Once the tumor volume was around 100 mm³, the mice were randomly divided into five groups (n = 5 per group) and treated with 5% glucose, free siRNA, CNPS, CN, and CNPPs, respectively, by intravenous injection every 2 days at a dose of 1.2 mg/kg converting to siRNA. The tumor volume was measured daily and calculated based on the equation $(a \times b^2) / 2$, where “a” and “b” represent the length and width of the tumor, respectively. The body weights of animals were also monitored daily during the experimental period. The mice were sacrificed 24 hr after the final injection.

Pharmacokinetic and Biodistribution Study

To investigate the pharmacokinetic characteristics of siRNA in different formulations, male nude mice were randomly divided into four groups (five mice per group) and mice in each group received Cy7-labeled CNPPs, Cy7-labeled CNPS, Cy7-labeled CN, and Cy7-labeled siRNA, respectively, via tail vein injection at the siRNA dose of 0.125 mg/kg. Thereafter, retro-orbital blood samples (about 40 μ L) were collected in preheparinized tubes at 5 min, 10 min, 20 min, 30 min, 60 min, 120 min, 240 min, and 480 min. Blood samples were then transferred to tubes containing heparin and stored at -20°C until analysis. To determine the concentration of siRNA in blood, 20 μ L of blood were transferred to a black 96-well plate, and the sample was diluted 1.5 times in MilliQ water. Then, Cy7 fluorescence was measured on a PolarStar fluorimeter (BMG) at $\lambda_{\text{ex}} = 750$ nm and $\lambda_{\text{em}} = 773$ nm. Finally, the acquired values were normalized to a siRNA concentration calculated from calibration curves.⁵⁴

To obtain the detail biodistribution of siRNA in mice at different times, male nude mice bearing a MCF-7 tumor were randomly divided into four groups (12 mice per group) and intravenously administered Cy7-labeled CNPPs, Cy7-labeled CNPS, Cy7-labeled CN, and Cy7-labeled siRNA, respectively, at the siRNA dose of 0.125 mg/kg. At 1 hr, 4 hr, 8 hr, and 24 hr post-injection, three mice in each group were sacrificed. The main organs (heart, liver, spleen, lung, and kidney) and tumors were simultaneously excised and stored at -80°C until analysis. To compare drug distribution in the tumor model with low expression of a transferrin receptor, the distribution of Cy7-labeled preparations in male nude mice bearing a HT-1080 tumor were also investigated as that in male nude mice bearing a MCF-7 tumor. To determine siRNA accumulation, tissues were first placed for several minutes in liquid nitrogen, then homogenized using a homogenizer and lysed using $1 \times$ passive lysis buffer (PLB, Promega) (250 μ L for the spleen and heart, 500 μ L for the lung and kidney, and 1,000 μ L for the liver). Cy7-labeled siRNA fluorescence was measured with the method used for pharmacokinetic analysis. The acquired values were normalized to protein content (Pierce) to get FU/mg.⁵⁴

Statistical Analysis

All data were shown as mean \pm SD. Student's t test or one-way ANOVA was used for the statistical evaluation. Differences between groups were considered as statistically significant when the probability (p) was less than 0.05.

AUTHOR CONTRIBUTIONS

Z.L. conceived the study, supervised experiments, and analyzed the data; L.L. designed the experiments and wrote the manuscript; X.H., M.Z., and S.M. performed the preparation, characterization, and in vitro evaluation of different formulations; F.Y., S.Z., N.L., and Z.W. conducted the experiments involving in vivo antitumor efficacy, pharmacokinetic, and biodistribution study; Y.W., H.G., and X.P. performed the in vivo imaging; Y.G., Y.Z., Y.L., Y.Y., X.T., M.L., and C.L. participated in the animal experiments; and X.M. revised the manuscript.

CONFLICTS OF INTEREST

The authors report no conflicts of interest.

ACKNOWLEDGMENTS

LetPub contributed linguistic assistance during the preparation of this manuscript, but this does not alter our adherence to policies on sharing data and materials. This work was supported by the Beijing Natural Science Foundation (no. 7144229, 2014) and the Natural Science Foundation of China (no. 81502675, 2016). We thank LetPub for its linguistic assistance during the preparation of this manuscript.

REFERENCES

- Fernández Fernández, E., Santos-Carballal, B., Weber, W.M., and Goycoolea, F.M. (2016). Chitosan as a non-viral co-transfection system in a cystic fibrosis cell line. *Int. J. Pharm.* 502, 1–9.
- Ragelle, H., Riva, R., Vandermeulen, G., Naeye, B., Pourcelle, V., Le Duff, C.S., D'Haese, C., Nysten, B., Braeckmans, K., De Smedt, S.C., et al. (2014). Chitosan nanoparticles for siRNA delivery: optimizing formulation to increase stability and efficiency. *J. Control. Release* 176, 54–63.
- Al-Qadi, S., Grenha, A., and Remuñán-López, C. (2012). Chitosan and its derivatives as nanocarriers for siRNA delivery. *J. Drug Deliv. Sci. Technol.* 22, 29–42.
- Lee, S.J., Kim, M.J., Kwon, I.C., and Roberts, T.M. (2016). Delivery strategies and potential targets for siRNA in major cancer types. *Adv. Drug Deliv. Rev.* 104, 2–15.
- Conde, J., Ambrosone, A., Hernandez, Y., Tian, F., McCully, M., Berry, C.C., Baptista, P.V., Tortiglione, C., and de la Fuente, J.M. (2015). 15 years on siRNA delivery: beyond the state-of-the-art on inorganic nanoparticles for RNAi therapeutics. *Nano Today* 10, 421–450.
- Kim, H.J., Kim, A., Miyata, K., and Kataoka, K. (2016). Recent progress in development of siRNA delivery vehicles for cancer therapy. *Adv. Drug Deliv. Rev.* 104, 61–77.
- Shu, Y., Cinier, M., Shu, D., and Guo, P. (2011). Assembly of multifunctional phi29 pRNA nanoparticles for specific delivery of siRNA and other therapeutics to targeted cells. *Methods* 54, 204–214.
- Guo, P., Coban, O., Snead, N.M., Trebley, J., Hoepflich, S., Guo, S., and Shu, Y. (2010). Engineering RNA for targeted siRNA delivery and medical application. *Adv. Drug Deliv. Rev.* 62, 650–666.
- Ma, Y., Nolte, R.J., and Cornelissen, J.J. (2012). Virus-based nanocarriers for drug delivery. *Adv. Drug Deliv. Rev.* 64, 811–825.
- Santel, A., Aleku, M., Keil, O., Endruschat, J., Esche, V., Fisch, G., Dames, S., Löffler, K., Fechtner, M., Arnold, W., et al. (2006). A novel siRNA-lipoplex technology for RNA interference in the mouse vascular endothelium. *Gene Ther.* 13, 1222–1234.

11. Landen, C.N., Jr., Chavez-Reyes, A., Bucana, C., Schmandt, R., Deavers, M.T., Lopez-Berestein, G., and Sood, A.K. (2005). Therapeutic EphA2 gene targeting in vivo using neutral liposomal small interfering RNA delivery. *Cancer Res.* 65, 6910–6918.
12. Bao, Y., Jin, Y., Chivukula, P., Zhang, J., Liu, Y., Liu, J., Clamme, J.P., Mahato, R.I., Ng, D., Ying, W., et al. (2013). Effect of PEGylation on biodistribution and gene silencing of siRNA/lipid nanoparticle complexes. *Pharm. Res.* 30, 342–351.
13. Davis, M.E. (2009). The first targeted delivery of siRNA in humans via a self-assembling, cyclodextrin polymer-based nanoparticle: from concept to clinic. *Mol. Pharm.* 6, 659–668.
14. Urban-Klein, B., Werth, S., Abuharbeid, S., Czubyko, F., and Aigner, A. (2005). RNAi-mediated gene-targeting through systemic application of polyethylenimine (PEI)-complexed siRNA in vivo. *Gene Ther.* 12, 461–466.
15. Mao, C.Q., Du, J.Z., Sun, T.M., Yao, Y.D., Zhang, P.Z., Song, E.W., and Wang, J. (2011). A biodegradable amphiphilic and cationic triblock copolymer for the delivery of siRNA targeting the acid ceramidase gene for cancer therapy. *Biomaterials* 32, 3124–3133.
16. Mao, C.Q., Xiong, M.H., Liu, Y., Shen, S., Du, X.J., Yang, X.Z., Dou, S., Zhang, P.Z., and Wang, J. (2014). Synthetic lethal therapy for KRAS mutant non-small-cell lung carcinoma with nanoparticle-mediated CDK4 siRNA delivery. *Mol. Ther.* 22, 964–973.
17. Shen, S., Mao, C.Q., Yang, X.Z., Du, X.J., Liu, Y., Zhu, Y.H., and Wang, J. (2014). Cationic lipid-assisted polymeric nanoparticle mediated GATA2 siRNA delivery for synthetic lethal therapy of KRAS mutant non-small-cell lung carcinoma. *Mol. Pharm.* 11, 2612–2622.
18. El-Andaloussi, S., Lee, Y., Lakhali-Littleton, S., Li, J., Seow, Y., Gardiner, C., Alvarez-Erviti, L., Sargent, I.L., and Wood, M.J. (2012). Exosome-mediated delivery of siRNA in vitro and in vivo. *Nat. Protoc.* 7, 2112–2126.
19. Alvarez-Erviti, L., Seow, Y., Yin, H., Betts, C., Lakhali, S., and Wood, M.J. (2011). Delivery of siRNA to the mouse brain by systemic injection of targeted exosomes. *Nat. Biotechnol.* 29, 341–345.
20. Lee, H., Lytton-Jean, A.K., Chen, Y., Love, K.T., Park, A.I., Karagiannis, E.D., Sehgal, A., Querbes, W., Zurenko, C.S., Jayaraman, M., et al. (2012). Molecularly self-assembled nucleic acid nanoparticles for targeted in vivo siRNA delivery. *Nat. Nanotechnol.* 7, 389–393.
21. Goodman, R.P., Schaap, I.A., Tardin, C.F., Erben, C.M., Berry, R.M., Schmidt, C.F., and Turberfield, A.J. (2005). Rapid chiral assembly of rigid DNA building blocks for molecular nanofabrication. *Science* 310, 1661–1665.
22. Schwartz, C., and Guo, P. (2013). Ultrastable pRNA hexameric ring gearing hexameric phi29 DNA-packaging motor by revolving without rotating and coiling. *Curr. Opin. Biotechnol.* 24, 581–590.
23. Zhou, J., Shu, Y., Guo, P., Smith, D.D., and Rossi, J.J. (2011). Dual functional RNA nanoparticles containing phi29 motor pRNA and anti-gp120 aptamer for cell-type specific delivery and HIV-1 inhibition. *Methods* 54, 284–294.
24. Guo, S., Huang, F., and Guo, P. (2006). Construction of folate-conjugated pRNA of bacteriophage phi29 DNA packaging motor for delivery of chimeric siRNA to nasopharyngeal carcinoma cells. *Gene Ther.* 13, 814–820.
25. Khaled, A., Guo, S., Li, F., and Guo, P. (2005). Controllable self-assembly of nanoparticles for specific delivery of multiple therapeutic molecules to cancer cells using RNA nanotechnology. *Nano Lett.* 5, 1797–1808.
26. Haque, F., Shu, D., Shu, Y., Shlyakhtenko, L.S., Rychahou, P.G., Evers, B.M., and Guo, P. (2012). Ultrastable synergistic tetraivalent RNA nanoparticles for targeting to cancers. *Nano Today* 7, 245–257.
27. Shu, Y., Pi, F., Sharma, A., Rajabi, M., Haque, F., Shu, D., Leggas, M., Evers, B.M., and Guo, P. (2014). Stable RNA nanoparticles as potential new generation drugs for cancer therapy. *Adv. Drug Deliv. Rev.* 66, 74–89.
28. Li, L., Liu, J., Diao, Z., Shu, D., Guo, P., and Shen, G. (2009). Evaluation of specific delivery of chimeric phi29 pRNA/siRNA nanoparticles to multiple tumor cells. *Mol. Biosyst.* 5, 1361–1368.
29. Zhang, H., Endrizzi, J.A., Shu, Y., Haque, F., Sauter, C., Shlyakhtenko, L.S., Lyubchenko, Y., Guo, P., and Chi, Y.I. (2013). Crystal structure of 3WJ core revealing divalent ion-promoted thermostability and assembly of the Phi29 hexameric motor pRNA. *RNA* 19, 1226–1237.
30. Rudzinski, W.E., and Aminabhavi, T.M. (2010). Chitosan as a carrier for targeted delivery of small interfering RNA. *Int. J. Pharm.* 399, 1–11.
31. Ragelle, H., Vandermeulen, G., and Préat, V. (2013). Chitosan-based siRNA delivery systems. *J. Control. Release* 172, 207–218.
32. Hoshyar, N., Gray, S., Han, H., and Bao, G. (2016). The effect of nanoparticle size on in vivo pharmacokinetics and cellular interaction. *Nanomedicine (Lond.)* 11, 673–692.
33. Kulkarni, S.A., and Feng, S.S. (2013). Effects of particle size and surface modification on cellular uptake and biodistribution of polymeric nanoparticles for drug delivery. *Pharm. Res.* 30, 2512–2522.
34. Hu, J., Xiao, F., Hao, X., Bai, S., and Hao, J. (2014). Inhibition of monocyte adhesion to brain-derived endothelial cells by dual functional RNA chimeras. *Mol. Ther. Nucleic Acids* 3, e209.
35. Xie, Y., Qiao, H., Su, Z., Chen, M., Ping, Q., and Sun, M. (2014). PEGylated carboxymethyl chitosan/calcium phosphate hybrid anionic nanoparticles mediated hTERT siRNA delivery for anticancer therapy. *Biomaterials* 35, 7978–7991.
36. Yang, Y., Yang, Y., Xie, X., Wang, Z., Gong, W., Zhang, H., Li, Y., Yu, F., Li, Z., and Mei, X. (2015). Dual-modified liposomes with a two-photon-sensitive cell penetrating peptide and NGR ligand for siRNA targeting delivery. *Biomaterials* 48, 84–96.
37. Chan, P., Kurisawa, M., Chung, J.E., and Yang, Y.Y. (2007). Synthesis and characterization of chitosan-g-poly(ethylene glycol)-folate as a non-viral carrier for tumor-targeted gene delivery. *Biomaterials* 28, 540–549.
38. van Steenis, J.H., van Maarseveen, E.M., Verbaan, F.J., Verrijck, R., Crommelin, D.J., Storm, G., and Hennink, W.E. (2003). Preparation and characterization of folate-targeted pEG-coated pDMAEMA-based polyplexes. *J. Control. Release* 87, 167–176.
39. Chen, C., Sheng, S., Shao, Z., and Guo, P. (2000). A dimer as a building block in assembling RNA. A hexamer that gears bacterial virus phi29 DNA-translocating machinery. *J. Biol. Chem.* 275, 17510–17516.
40. Mat-Arip, Y., Garver, K., Chen, C., Sheng, S., Shao, Z., and Guo, P. (2001). Three-dimensional interaction of phi29 pRNA dimer probed by chemical modification interference, cryo-AFM, and cross-linking. *J. Biol. Chem.* 276, 32575–32584.
41. Katas, H., and Alpar, H.O. (2006). Development and characterisation of chitosan nanoparticles for siRNA delivery. *J. Control. Release* 115, 216–225.
42. Rudzinski, W.E., Palacios, A., Ahmed, A., Lane, M.A., and Aminabhavi, T.M. (2016). Targeted delivery of small interfering RNA to colon cancer cells using chitosan and PEGylated chitosan nanoparticles. *Carbohydr. Polym.* 147, 323–332.
43. Zeng, C., Yu, F., Yang, Y., Cheng, X., Liu, Y., Zhang, H., Zhao, S., Yang, Z., Li, M., Li, Z., and Mei, X. (2016). Preparation and evaluation of oxaliplatin thermosensitive liposomes with rapid release and high stability. *PLoS ONE* 11, e0158517.
44. Ragelle, H., Colombo, S., Pourcelle, V., Vanvarenberg, K., Vandermeulen, G., Bouzin, C., Marchand-Brynaert, J., Feron, O., Foged, C., and Préat, V. (2015). Intracellular siRNA delivery dynamics of integrin-targeted, PEGylated chitosan-poly(ethylene imine) hybrid nanoparticles: A mechanistic insight. *J. Control. Release* 211, 1–9.
45. Xiao, B., Ma, P., Viennois, E., and Merlin, D. (2016). Urocanic acid-modified chitosan nanoparticles can confer anti-inflammatory effect by delivering CD98 siRNA to macrophages. *Colloids Surf. B Biointerfaces* 143, 186–193.
46. Chen, C.H., Dellamaggiore, K.R., Ouellette, C.P., Sedano, C.D., Lizadjohry, M., Chernis, G.A., Gonzales, M., Baltasar, F.E., Fan, A.L., Myerowitz, R., and Neufeld, E.F. (2008). Aptamer-based endocytosis of a lysosomal enzyme. *Proc. Natl. Acad. Sci. USA* 105, 15908–15913.
47. Eltayeb, S.E., Su, Z., Xiao, Y., and Ping, Q. (2016). Antitumor activity of transferrin-modified-atomer lipid nanospheres in cancer cell lines. *J. Drug Deliv. Sci. Technol.* 31, 118–129.
48. Chen, J., Lu, S., Gu, W., Peng, P., Dong, J., Xu, F., Yang, X., Xiong, Z., and Yang, X. (2015). Characterization of 9-nitrocamptothecin-in-cyclodextrin-in-liposomes modified with transferrin for the treating of tumor. *Int. J. Pharm.* 490, 219–228.
49. Malarvizhi, G.L., Retnakumari, A.P., Nair, S., and Koyakutty, M. (2014). Transferrin targeted core-shell nanomedicine for combinatorial delivery of doxorubicin and sorafenib against hepatocellular carcinoma. *Nanomedicine (Lond.)* 10, 1649–1659.
50. Darvishi, M.H., Nomani, A., Amini, M., Shokrgozar, M.A., and Dinarvand, R. (2013). Novel biotinylated chitosan-graft-polyethylenimine copolymer as a targeted non-viral vector for anti-EGF receptor siRNA delivery in cancer cells. *Int. J. Pharm.* 456, 408–416.

51. Lee, D.W., Yun, K.S., Ban, H.S., Choe, W., Lee, S.K., and Lee, K.Y. (2009). Preparation and characterization of chitosan/polyguluronate nanoparticles for siRNA delivery. *J. Control. Release* 139, 146–152.
52. Liu, X., Howard, K.A., Dong, M., Andersen, M.Ø., Rahbek, U.L., Johnsen, M.G., Hansen, O.C., Besenbacher, F., and Kjems, J. (2007). The influence of polymeric properties on chitosan/siRNA nanoparticle formulation and gene silencing. *Biomaterials* 28, 1280–1288.
53. Noh, S.M., Park, M.O., Shim, G., Han, S.E., Lee, H.Y., Huh, J.H., Kim, M.S., Choi, J.J., Kim, K., Kwon, I.C., et al. (2010). Pegylated poly-L-arginine derivatives of chitosan for effective delivery of siRNA. *J. Control. Release* 145, 159–164.
54. Aldrian, G., Vaissière, A., Konate, K., Seisel, Q., Vivès, E., Fernandez, F., Viguier, V., Genevois, C., Couillaud, F., Démèné, H., et al. (2017). PEGylation rate influences peptide-based nanoparticles mediated siRNA delivery in vitro and in vivo. *J. Control. Release* 256, 79–91.